28 GHz Over-the-Air Measurement using an OTFS Multi-User Distributed MIMO

Noriaki Tawa, Toshihide Kuwabara, Yasushi Maruta, Tomoya Kaneko

NEC Corporation, Kawasaki, Kanagawa, 211-8666, Japan

{n-tawa, t-kuwa, y-maruta, tomoyakaneko}@nec.com

***Abstract* — This paper describes the experimental investigation of orthogonal time frequency space (OTFS) modulation using a 28 GHz multi-user distributed multiple-input multiple-output (D-MIMO) testbed in over-the-air (OTA) and mobility environments. We build the D-MIMO testbed in an actual office floor, and measure OTFS signals and orthogonal frequency-division multiplexing (OFDM) signals with up to four user simultaneous connections. OTFS indicates higher robustness in time-variant channels than OFDM. The error vector magnitude (EVM) and system throughput of OTFS are −22 dB and 1.9 Gbps with 100 MHz signal bandwidth, respectively. In our knowledge, this is a first paper describing the OTA measurements of EVM, throughput, and spectral efficiency using OTFS modulation on the 28 GHz coherent beamforming system.**

***Keywords* — OTFS, channel estimation, MIMO, Mobile communication, millimeter wave communication.**

I. INTRODUCTION

The enhancement of cell throughput is a key requirement in recent mobile communications, such as 5G or later. Multiple-input multiple-output (MIMO) techniques, using millimeter-wave (mmWave) band, and new modulation scheme are important to enhance the cell throughput significantly. Spatial division multiplexing (SDM) is one of the MIMO techniques and can multiple the larger number of layers by using null steering than direction based beam-forming. The benefits of using mmWave are wide available frequency range, whereas its difficulties are varying propagation channels more sensitively in mmWave than in sub-6 GHz. The modulation technique for 4G and 5G is orthogonal frequency-division multiplexing (OFDM). Although OFDM has high spectral efficiency and good robustness in multi-path fading, inter-carrier interference due to the Doppler spread of time-varying channels degrades OFDM performance for mobility environments. Especially, Doppler spread in mmWave is larger than that in sub-6 GHz. To suppress the degradation, OFDM system allocates reference signals (RS) more frequently and needs to calculate SDM weight matrixes for each OFDM symbol. However, increasing RS allocations decreases spectral efficiency and increases computational complexity for weight calculation drastically.

Orthogonal time frequency space (OTFS) is suggested to tackle the time-varying channels [1]. OFDM multiplexes information symbols in the frequency-time (FT) domain, whereas OTFS multiplexes them in the delay-Doppler (DD) domain. Because the OTFS modulation spreads each element in the DD grid into the FT domain entirely, all OTFS elements experience the same and nearly constant propagation channel. Using simulation, previous works report that OTFS has a higher bit error rate than OFDM for high mobility environments [1]–[3].

We investigate the robustness of OTFS modulation in the Doppler environment with over-the-air (OTA) experiments using a 28 GHz multi-user distributed MIMO (D-MIMO) testbed. D-MIMO is one of the technique to maximize the SDM performance by using geometrically distant multiple number of antennas [4], [5]. This paper describes the practical OTFS channel estimation and channel quality with simultaneous multiple user connections for mobility environments.

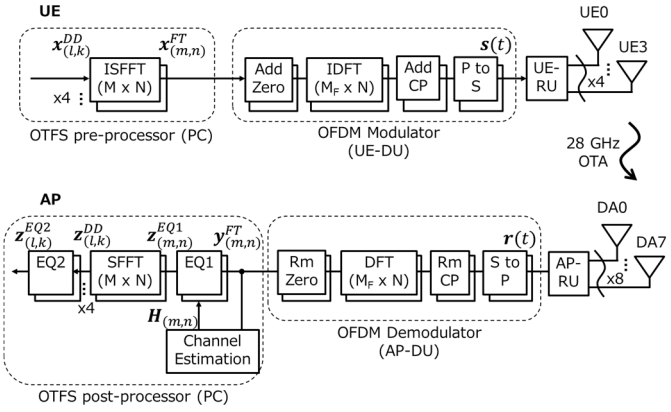

Fig. 1. Block diagram of OTFS signal processing.

II. SIGNAL PROCESSING

A. OTFS Modulation

Figure 1 shows the OTFS signal processing diagram. An OTFS pre-processor on a PC generates a multi-user transmitted (TX) signal $\boldsymbol{x}^{\mathrm{DD}}_{(l,k)} \in \mathbb{C}^{U\times 1}$, where $U = 1, 2, \text{or } 4$ is the number of user equipments (UEs), allocated in the DD domain with a delay domain index $l = 0, 1, \ldots, M-1$ and a Doppler domain index $k = 0, 1, \ldots, N-1$. The values of M and N are 1200 and 14, respectively. The OTFS signal $\boldsymbol{x}^{\mathrm{DD}}_{(l,k)}$ is an element in an OTFS subframe, and an OTFS frame has 10 OTFS subframes. The OTFS pre-processor converts $\boldsymbol{x}^{\mathrm{DD}}_{(l,k)}$ to a

FT domain signal $\boldsymbol{x}^{\mathrm{FT}}_{(m,n)} \in \mathbb{C}^{U\times 1}$, where $m = 0, 1, \ldots, M-1$ is a frequency domain index and $k = 0, 1, \ldots, N-1$ is a time domain index, with inverse symplectic finite Fourier transform (ISFFT) [1]–[3]. A distributed unit (DU) for UE, called UE-DU, generates a time domain digital signal $\boldsymbol{s}(t) \in \mathbb{C}^{U\times 1}$, where t is time from the beginning of a subframe, by modulating the TF domain signal $\boldsymbol{x}^{\mathrm{FT}}_{(m,n)}$ with the OFDM modulation. The numerology of the OFDM modulation is based on the specifications of 3GPP TS 36.211 format [6] except for subcarrier spacing and signal bandwidth, which use 60 kHz and 80 MHz respectively. A radio unit (RU) for UE, called UE-RU, converts the time domain digital signal $\boldsymbol{s}(t)$ to an analogue signal and then radiates it from UE antennas.

The first OTFS subframe has only reference signals to estimate a channel impulse response (CIR), which is called CIR-RS. CIR-RS uses the root Zadoff-chu sequence with a length of 19 as defined in 3GPP TS 36.211 [6] and is allocated to the DD domain grids as shown in Fig. 2. Table 1 shows delay indexes $l_{c,u}$ and Doppler indexes $k_{c,u}$ for the CIR-RS centre locations of four UEs, UE0 to UE3. The other grids in the first subframe are blank. The second to tenth subframes have quadrature phase shift keying (QPSK) TX information and phase compensation reference signals (PCRS). PCRS for the u-th UE is a QPSK sequence and is allocated to $\boldsymbol{x}^{\mathrm{DD}}_{(lp,0)}$, where $l_p = 48v + u$, $v = 0, 1, \ldots, 24$, and $u = 0, 1, 2, 3$, as shown in Fig. 2. PCRS and CIR-RS locations are different for each UE to prevent contamination of the reference signals between UEs. The amplitude of CIR-RS is 17 dB larger than those of the TX information sequence and PCRS to equalize the peak power of the time domain signal $\boldsymbol{s}(t)$ between the first subframe and the other subframes as shown in Fig. 3.

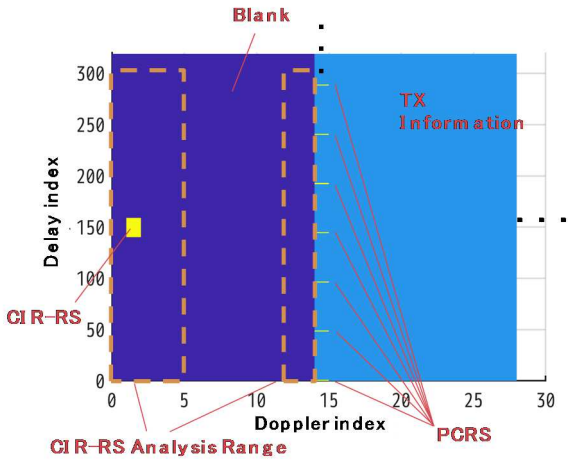

Fig. 2. OTFS signal allocation for UE0 from the first subframe to the second subframe.

B. OTFS demodulator

A DU for access point (AP), called AP-DU, generates a FT domain OTFS signal $\boldsymbol{y}^{\mathrm{FT}}_{(m,n)} \in \mathbb{C}^{D\times 1}$, where $D = 8$ is the number of distributed antennas (DAs), from the time domain signal $\boldsymbol{r}(t) \in \mathbb{C}^{D\times 1}$ received by an RU for AP (AP-RU) with the OFDM demodulation.

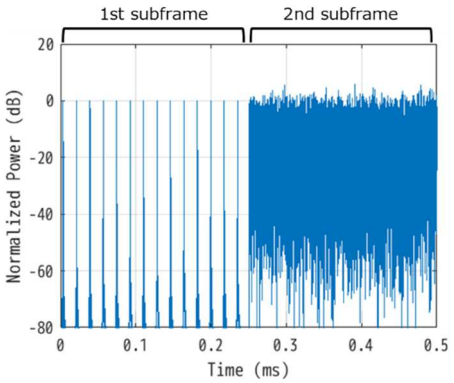

Fig. 3. Time domain OTFS waveform for UE0.

Table 1. Numerology for CIR-RS.

	UE0	UE1	UE2	UE3
Length of CIR-RS	19	19	19	19
Centre of CIR-RS				
Delay index $l_{c,u}$	150	750	450	1050
Doppler index $k_{c,u}$	1	9	5	12
CIR-RS analysis range				
Delay domain $l_{r,u}$	150	150	150	150
Doppler domain $k_{r,u}$	3 (walk) 0 (stop)	0	0	0

The propagation channels are estimated by using the first subframe having CIR-RS. Firstly, the channel estimator in the OTFS post-processor converts the FT domain subframe $\boldsymbol{y}^{\mathrm{FT}}_{(m,n)}$ to the DD domain subframe $\boldsymbol{y}^{\mathrm{DD}}_{(l,k)} \in \mathbb{C}^{D\times 1}$ with SFFT, and then extracts CIR-RS from $\boldsymbol{y}^{\mathrm{DD}}_{(l,k)}$. The extracted signal $\boldsymbol{e}^{\mathrm{DD}}_{u(l,k)} \in \mathbb{C}^{D\times 1}$ for the u-th UE is expressed as

$$\boldsymbol{e}^{\mathrm{DD}}_{u(l,k)} = \begin{cases} \boldsymbol{y}^{\mathrm{DD}}_{(l,k)}, & l_{c,u} - l_{r,u} \le l \le l_{c,u} + l_{r,u} \\ & k_{c,u} - k_{r,u} \le k \le k_{c,u} + k_{r,u} \\ 0, & l < l_{c,u} - l_{r,u}, l > l_{c,u} + l_{r,u} \\ & k < k_{c,u} - k_{r,u}, k > k_{c,u} + k_{r,u} \end{cases}, \quad (1)$$

where $l_{r,u}$ and $k_{r,u}$ are the CIR-RS analysis ranges of delay domain and Doppler domain, respectively, as shown in Table 1. The CIR-RS analysis range is larger than the CIR-RS allocations range because CIR-RS is distributed by delay and Doppler effects. When the Doppler indexes of CIR-RS analysis range are over the first subframe, the indexes are folded in the first subframe as shown in Fig. 2. The channel estimator converts the extracted signal $\boldsymbol{e}^{\mathrm{DD}}_{u(l,k)}$ to the TF domain signal $\boldsymbol{e}^{\mathrm{TF}}_{u(m,n)} \in \mathbb{C}^{D\times 1}$ with ISFFT and calculates the propagation channel of the u-th UE, $\boldsymbol{h}_{u(m,n)}$, as

$$\boldsymbol{h}_{u(m,n)} = \boldsymbol{e}^{\mathrm{TF}}_{u(m,n)} / x^{\mathrm{TF}}_{u(m,n)}, \quad (2)$$

where, $x^{\mathrm{TF}}_{u(m,n)}$ is the FT domain TX signal of the u-th UE in $\boldsymbol{x}^{\mathrm{TF}}_{(m,n)}$ of the first subframe. The channel estimator obtains the channel matrix $\boldsymbol{H}_{(m,n)} = [\boldsymbol{h}_{0(m,n)}, \boldsymbol{h}_{1(m,n)}, \ldots, \boldsymbol{h}_{U-1(m,n)}]$.

The first equalizer (EQ1) performs equalization in the FT domain. The equalized OTFS signal, $\boldsymbol{z}_{(m,n)}^{\mathrm{EQ1}} \in \mathbb{C}^{U\times 1}$, is calculated as

$$\boldsymbol{z}_{(m,n)}^{\mathrm{EQ1}} = \boldsymbol{W}_{(m,n)}\boldsymbol{y}_{(m,n)}^{\mathrm{FT}}, \tag{3}$$

where $\boldsymbol{W}_{(m,n)} \in \mathbb{C}^{U\times D}$ is the equalization weight calculated from the channel matrix $\boldsymbol{H}_{(m,n)}$ by zero-forcing (ZF). Subsequently, the OTFS post-processor converts the equalized signal $\boldsymbol{z}_{(m,n)}^{\mathrm{EQ1}}$ to the DD domain signal $\boldsymbol{z}_{(l,k)}^{\mathrm{DD}} \in \mathbb{C}^{U\times 1}$ with SFFT.

In the Doppler environments of frequency shift f_o Hz, the received (RX) time domain signal $r(t)$ in the a-th subframe is easily expressed as,

$$r(t) = s(t)\exp\{j2\pi f_o(aT + t)\}, \tag{4}$$

where $s(t)$ is the transmitted time domain signal, and $T = 0.25$ ms is the time length of a subframe. The RX signal $r(t)$ is constantly rotated with $\exp(j2\pi f_o aT)$. The OTFS post-processor extrapolates the channels of the first subframe to the other subframes in a frame, and thus needs to correct the differences between subframes such as shown in (4). The second equalizer (EQ2) corrects the differences as follows,

$$\boldsymbol{z}_{(l,k)}^{\mathrm{EQ2}} = \boldsymbol{z}_{(l,k)}^{\mathrm{DD}} \odot \boldsymbol{c}, \tag{5}$$

where

$$\boldsymbol{c} = \frac{1}{N_{lp}}\sum_{l\in l_p} \boldsymbol{x}_{(l,0)}^{\mathrm{DD}} \oslash \boldsymbol{z}_{(l,0)}^{\mathrm{DD}}, \tag{6}$$

and $N_{lp} = 25$ is the number of PCRSs. The symbols of $\odot$ and $\oslash$ denote the Hadamard product and division, respectively.

III. Over the Air Measurement

A. 28 GHz D-MIMO Testbed

Figure 4 shows the block diagram of a 28 GHz base station AP RU that consists of the mixed signal processing (MSP) unit and eight DAs.

MSP has a field-programmable array of Xilinx ZU29DR that integrates eight analog-to-digital converters (ADCs) and eight digital-to-analog converters (DACs). The DACs generate TX intermediate frequency (IF) signals, and the ADCs receives RX IF signals directly. MSP and DAs have newly designed sextuple multiplexers, which multiple a TX IF signal, a RX IF signal, a 3.3 GHz local oscillator (LO) signal, a time division duplex control signal, a radio frequency (RF) integrated circuit (IC) control signal, and 24 V direct current power. Thus, MSP can connect each DA using a single coaxial cable, which has up to 20 m length. The frequency of TX and RX IF signals is 1.5 GHz to decrease cable losses.

DA converts between the IF signals and 28.25 GHz RF signals by mixing with a LO signal produced by eight times of an original 3.3 GHz signal. Each DA has eight element waveguide array antenna having element intervals of half wave length at 28 GHz. The eight antenna elements connect to the eight channel bi-directional transceiver IC based on 65 nm CMOS integrating gain and phase shifters [7]. The measured effective isotropic radiated power of DA is 22 dBm.

B. Measurement Setup

Figure 5 shows the experimental layout of eight DAs, DA0 to DA7, and four UEs, UE0 to UE3, in an office floor. The heights of DAs and UEs are about 1.7 m from the floor. The UE system have the same architecture as the AP D-MIMO system except for the number of antenna units, and thus UEs can be located at arbitrary places in the floor. UE0 is used for single user measurements, and UE0 and UE1 are used for two user multiplexing. Our measurements have two parts as follows. In the part-1, UE0 moves to left direction in Fig. 5 at walking speed (~4 km/h), whereas the other UEs are fixed at the initial locations. Because CIR is spread in Doppler domain for mobility environments, the CIR-RS analysis range of Doppler domain for UE0, $k_{r,u=0}$, is three as shown in Table 1. The CIR-RS analysis ranges $k_{r,u}$ for the other UEs are zero to decrease additive white Gaussian noise contaminated to the CIR estimation. In the part-2, all UEs are fixed at the initial locations, and their CIR-RS analysis ranges $k_{r,u}$ are zero.

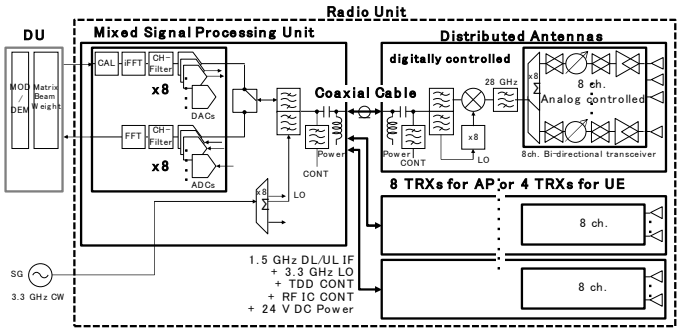

Fig. 4. Block diagram of the D-MIMO system.

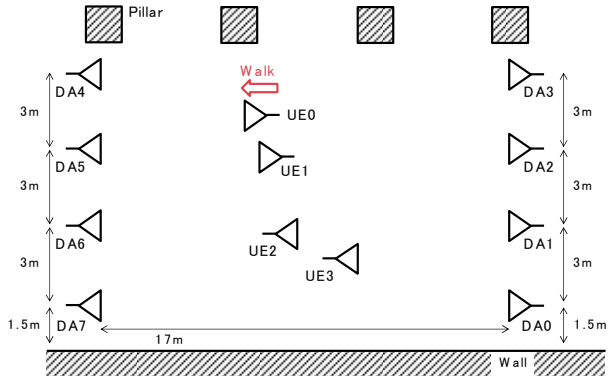

Fig. 5. Experimental layout on the office floor. The Antenna directions of DAs and UEs are correspond to the directions of antenna symbols.

IV. Measurement Result and Discussion

Figure 6 shows the UE0 OTFS constellations in the part-1 measurements. Although the constellation without using EQ2 shown in Fig. 6(a) is rotated for each subframe by Doppler frequency shift, the constellation using EQ2 shown in Fig.

6(b) is corrected for the rotation. Figure 7 shows the measured error vector magnitudes (EVMs) as a function of the number of simultaneously connected UEs. AP D-MIMO can demodulate the multi-user OTFS signals, which are emitted in the same frequency band and the same time, with ZF in the actual OTA and Doppler environments. In the part-2 measurements, which all UEs are fixed, the OTFS EVMs are about the same as the OFDM EVMs regardless of the number of connected UEs. In contrast, the EVMs of the moving OTFS UE0 in the part-1 measurements are several dB less than those of the moving OFDM UE0, which is shown by the blue solid circles in Fig. 7. The dark green solid circle in Fig. 7(b) shows the EVMs of the moving OFDM UE0 using phase tracking reference signals (PTRS). PTRS is based on the specifications in 3GPP TS 38.211 [8], which is allocated for each 48 subcarriers intervals in fourth to 14th OFDM symbols for each subframe. The OFDM EVMs of UE1 to UE3 with PTRS are about the same as those without PTRS because these UEs are fixed. Although the moving OFDM UE0 with PTRS has less EVM than the moving OTFS UE0, computational complexity for equalizations increases drastically to use PTRS. The channel equalizer for OFDM without using PTRS updates the equalization weights for each subframe, whereas that using PTRS updates the equalization weights for each OFDM symbol.

Table 2 shows comparison with the previously reported OTFS and OFDM systems without using PTRS. The system throughput (STP) and spectral efficiency of this work are estimated from the UE0 EVMs in the part-1 measurements by using MATLAB 5G toolbox. The STP is sum of four user throughputs with 100 MHz bandwidth signals. The experimentally estimated spectral efficiencies of this work are compatible with those of the previous work [9] calculated by simulation.

V. Conclusion

This paper has presented experimental investigation of OTFS performances using the 28 GHz D-MIMO testbed in OTA and mobility environments. We have built the D-MIMO testbed and have measured EVM with up to four user simultaneous connections in the actual office floor. In our knowledge, this is a first experimental verification of EVM, throughput, and spectral efficiency using OTFS modulation in 28 GHz OTA environments.

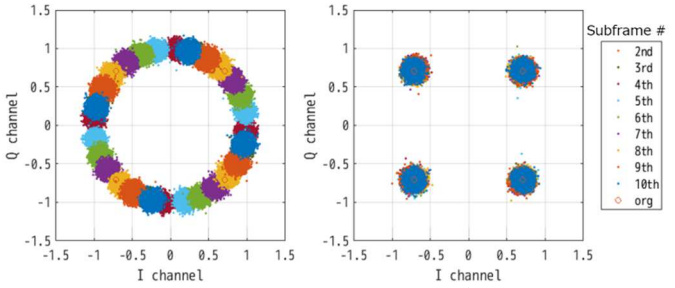

(a) (b)

Fig. 6. Measured UE0 OTFS QPSK constellations (a) without using EQ2 and (b) using EQ2.

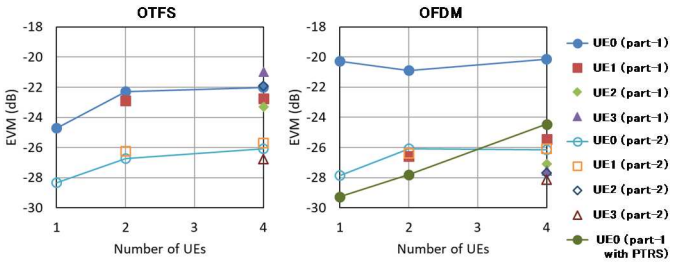

(a) (b)

Fig. 7. Measured EVMs as a function of the number of UEs with (a) OTFS and (b) OFDM.

Table 2. Comparison with the previously reported OTFS system.

Ref.	Experiment	Ant. config.	Mod. scheme	STP (Gbps)	Spectral eff. (bps/Hz)
Fig. 13 in [9]	Sim.	4×4	OFDM	–	14
	Sim.	4×4	OTFS	–	18
This work	Yes	4×8	OFDM	1.79	17.9
	Yes	4×8	OTFS	1.93	19.3

OTFS has had less EVM and higher spectral efficiency than OFDM without PTRS for moving UE and has achieved higher robustness in time-variant channels. These findings suggest that OTFS is one of the key technology to realize the 5G or later mobile communication systems used for high mobility environments and in high frequency range such as mmWave.

References

[1] R. Hadani et al., "Orthogonal Time Frequency Space Modulation," *2017 IEEE Wireless Communications and Networking Conference (WCNC)*, 2017, pp. 1-6.

[2] R. Hadani et al., "Orthogonal Time Frequency Space (OTFS) modulation for millimeter-wave communications systems," *2017 IEEE MTT-S International Microwave Symposium (IMS)*, 2017, pp. 681-683.

[3] W. Shen, L. Dai, J. An, P. Fan and R. W. Heath, "Channel Estimation for Orthogonal Time Frequency Space (OTFS) Massive MIMO," in *IEEE Transactions on Signal Processing*, vol. 67, no. 16, pp. 4204-4217, 15 Aug.15, 2019.

[4] N. Tawa, T. Kuwabara, Y. Maruta and T. Kaneko, "Measuring Propagation Channel Variations and Reciprocity using 28 GHz Indoor Distributed Multi-user MIMO," *2020 IEEE Radio and Wireless Symposium (RWS)*, 2020, pp. 104-107.

[5] I. C. Sezgin et al., "A Low-Complexity Distributed-MIMO Testbed Based on High-Speed Sigma–Delta-Over-Fiber," in *IEEE Transactions on Microwave Theory and Techniques*, vol. 67, no. 7, pp. 2861-2872, July 2019.

[6] *Evolved Universal Terrestrial Radio Access (E-UTRA);* Physical channels and modulation, version 10.7.0, document 3GPP TS 36.211, February 2013.

[7] J. Pang et al., "A 28-GHz CMOS Phased-Array Beamformer Utilizing Neutralized Bi-Directional Technique Supporting Dual-Polarized MIMO for 5G NR," in *IEEE Journal of Solid-State Circuits*, vol. 55, no. 9, pp. 2371-2386, Sept. 2020.

[8] *NR;* Physical channels and modulation, version 15.8.0, document 3GPP TS 38.211, December 2019.

[9] *3GPP TSG RA WG1*, "OTFS Modulation Waveform and Reference Signals for New RAT," R1-162930, April 2016.